Journal of Solid State Chemistry **143,** 41–51 (1999)
Article ID jssc.1998.8067, available online at http://www.idealibrary.com on IDEAL®

The Phase Transitions between $H_{0.13}V_{0.13}Mo_{0.87}O_3 \cdot 0.26H_2O$ and MoO_3: An X-Ray, Thermal Analysis, and TEM Study

L. Dupont, D. Larcher, and M. Touboul

Laboratoire de Réactivité et Chimie des Solides, Université de Picardie Jules Verne, UPRES A 6007, 33 rue Saint-Leu, F-80039 Amiens Cedex, France

Received June 15, 1998; in revised form October 5, 1998; accepted October 19, 1998

Mixed vanadium-molybdenum oxide hydrates ($H_xV_xMo_{1-x}O_3 \cdot 0.26H_2O$ with $0.06 \leq x \leq 0.18$) have been synthesized by a soft chemistry method. The phase transitions from one of these hydrates ($x = 0.13$) to the final product MoO_3 have been studied by thermal analysis, X-ray powder diffraction, and transmission electron microscopy techniques. Both metastable and stable oxides have been observed. $H_{0.13}V_{0.13}Mo_{0.87}O_3 \cdot 0.26H_2O$ possesses a structure related to hexagonal MoO_3. Dehydration of the precursor leads to a metastable phase $H_{0.13}V_{0.13}Mo_{0.87}O_3$, with a structure similar to that of the hydrate. At 500°C this phase transforms into the metastable $V_{0.13}Mo_{0.87}O_{2.935}$, with a structure related to the orthorhombic MoO_3 structure. The heating of this last phase above 500°C induces a change from the metastable system to the stable binary (V_2O_5–MoO_3) one. In agreement with this binary, a liquid phase and a solid phase with a composition closest to MoO_3, are formed during the phase segregation at 600°C. Models for explaining these phase transitions are proposed.

INTRODUCTION

One decade ago, an hydrated precursor $H_{0.13}V_{0.13}Mo_{0.87}O_3 \cdot 0.26H_2O$ isotypic with hexagonal MoO_3 (Fig. 1a) was synthesized using two different "chimie douce" methods by Davies *et al.* (1). The first approach (1–3) consists of the synthesis of an intermediary brannerite-type phase $LiVMoO_6$ by $LiVO_3$ and MoO_3 solid state reaction (4). This intermediary phase is soaked in hydrochloric acid solution, where it dissolves, and then the above-mentioned hydrated phase precipitates. In a second approach (5), lithiated mixed vanadium–molybdenum oxide hydrates isotypic with hexagonal MoO_3 structure are synthesized by dissolution of V_2O_5 and MoO_3 in LiOH aqueous solution or by dissolution of $LiVO_3$ and $Li_2Mo_2O_7$ in water. The so-obtained solutions are acidified and heated under reflux until the precipitation of phases with the chemical formula $(Li_xH_{0.13-x})(V_{0.13}Mo_{0.87})O_3 \cdot 0.26H_2O$ occurs. By ionic exchange in HCl at room temperature these phases transform into the pure protonic $H_{0.13}V_{0.13}Mo_{0.87}O_3 \cdot 0.26H_2O$ phase.

Recently, our research group reported a new way of obtaining not only the pure protonic hexagonal MoO_3 type oxide hydrate with the ratio $V/Mo = 0.13/0.87$ but also $H_xV_xMo_{1-x}O_3 \cdot nH_2O$ phases family with $0.06 \leq x \leq 0.18$ (6). The previously reported synthesis method (6) consists of the dissolution of metallic molybdenum and V_2O_5 in hydrogen peroxide solution. Then, the solution is heated until a yellow precipitate (the precursor) appears.

According to Davies *et al.* (5), the heating at 350°C of the hydrated precursor leads to $V_{0.13}Mo_{0.87}O_{2.935}$ with an hexagonal MoO_3 type structure (Fig. 1a), and this oxide is stable up to 460°C.

Nevertheless, questions remain concerning the behavior of this oxide heated above 460°C; does it transform into an orthorhombic double layer MoO_3 type structure oxide (Fig. 1b) or into a monoclinic MoO_3 type structure oxide (Fig. 1c)? Moreover, is the chemical formula $V_{0.13}Mo_{0.87}O_{2.935}$ in good agreement with an hexagonal MoO_3 type structure?

Based on our experience in the comprehension of phase transition mechanisms from hydrated transition metal oxide precursors synthesized by chimie douce, we decided to carry out the study of the phase transitions ensuing $H_{0.13}V_{0.13}Mo_{0.87}O_3 \cdot 0.26H_2O$ thermal treatment.

The present paper will describe how the phase transformations, from the $H_{0.13}V_{0.13}Mo_{0.87}O_3 \cdot 0.26H_2O$ precursor into the ultimate reaction product MoO_3, have been elucidated by a combination of thermal analysis methods, X-ray diffraction, and TEM techniques.

EXPERIMENTAL

A description of the synthesis method has already been given in detail (6). X-ray diffraction studies were done with a Guinier-Lenné heating camera (ENRAF diffractis 581, Cu$K\alpha$1 radiation isolated by a monochromator, platinum grid, heating rate 0.1°C/min, film rate 1.5 mm/h, under air) and a D5000 Bragg-Brentano diffractometer (radiation Cu$K\alpha$1). The data were treated with Dicvol 91 (7), NBS/AIDS83 (8), and Fullprof (9) software in order to

0022-4596/99 $30.00

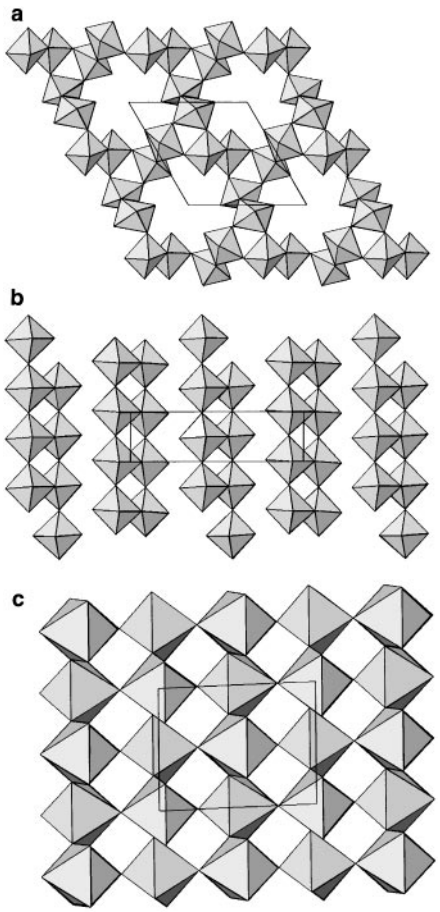

FIG. 1. Structures of polymorphic MoO_3 varieties. (a) Hexagonal MoO_3 along the [001] direction, (b) Orthorhombic MoO_3 along the [001] direction, (c) Monoclinic MoO_3 structure along the [010] direction.

determine the cell parameters of each phase. The X-ray results have been supplemented with simultaneous thermal analysis (STA): thermogravimetry (TG) and differential thermal analysis (DTA) on a SETARAM TG-DTA 92 (heating rate 5°C/min, under argon, open pan).

For the transmission electron microscopy (TEM) studies, a small amount of the particles was dispersed in 1-butanol by ultrasonic treatment. A drop of the suspension was collected on a holey carbon film supported on a Cu grid. The grids were studied in a JEOL JEM 200CX transmission electron microscope, equipped with a top-entry, double-tilt goniometer stage ($\pm 10°$), and operated at 200 kV for the high resolution electron microscopy studies. A JEOL JEM 2010 transmission electron microscope equipped with a GATAN eucentric goniometer ($\pm 40°$), complemented with an EDS analyzer (LINK ISIS) was used for electron diffraction (ED) study.

The scanning electron microscopy study was carried out with a PHILIPS XL30 FEG equipped with an EDS analyzer (LINK ISIS) in order to map the chemical composition of the particles.

The high resolution image simulations were calculated with EMS software (10).

RESULTS AND DISCUSSION

A. X-ray Diffraction and Thermal Analysis Studies

The X-ray powder diffraction pattern for $H_{0.13}V_{0.13}Mo_{0.87}O_3 \cdot 0.26H_2O$ has been indexed and used to obtain the following refined hexagonal unit cell parameters: $a = 10.6129(5)$ Å and $c = 3.7045(3)$ Å (6). The X-ray pattern looks like that of hexagonal MoO_3, with unit cell dimensions $a = 10.584$ Å, $c = 3.728$ Å and space group $P6_3$ (11). The slight difference in the parameters is most likely due to the difference in composition of the two compounds. The Guinier-Lenné X-ray photograph on Fig. 2 shows displacements and rearrangements of the diffraction lines due to structural transformations during heating of the precursor.

1. Hexagonal Mixed Vanadium–Molybdenum Trioxide, $H_{0.13}V_{0.13}Mo_{0.87}O_3$

The heating of the hydrated precursor to 300°C leads to the departure of the structural water contained in the tunnels. The large endothermic peak and the weight loss observed in region 1 (Fig. 3) correspond to the departure of this water. The tunnels are large enough to allow the departure of the structural water without any important modification of the structure skeleton. The so-obtained oxide presents the chemical composition $H_{0.13}V_{0.13}Mo_{0.87}O_3$. The unit cell parameters are close to those refined for the precursor. According to the X-ray diffraction pattern, the mixed hexagonal type structure oxide is stable up to 480°C (Fig. 2, region 2). From 300 to 480°C, the chemical composition of the oxide changes. The weight loss carries on (Fig. 3, region 2) without any evidence for a thermal phenomenon from the DTA curve. This weight loss could be attributed to the departure of protons, as water, by recombination with a part of the oxygen lattice. Close to 480°C, all protons leave the structure, and a phase transition occurs. All these observations evidence that the composition of the metastable mixed hexagonal type oxide varies according to the chemical formula $H_{0.13-x}V_{0.13}Mo_{0.87}O_{3-x/2}$ ($0 \leq x \leq 0.13$).

The departure of the protons leads to quantifiable unit cell parameters variations. A unit cell parameters refinement of an oxide treated up to 450°C leads to the following values: $a = 10.6033(8)$ Å, $c = 3.6970(3)$ Å. These values relate a slight decrease in the unit cell parameters compared to those of the precursor.

2. Orthorhombic Mixed Vanadium–Molybdenum Oxide, $V_{0.13}Mo_{0.87}O_{2.935}$

The X-ray diffraction pattern (Fig. 2, region 3) shows a structural change around 500°C. The mixed metastable

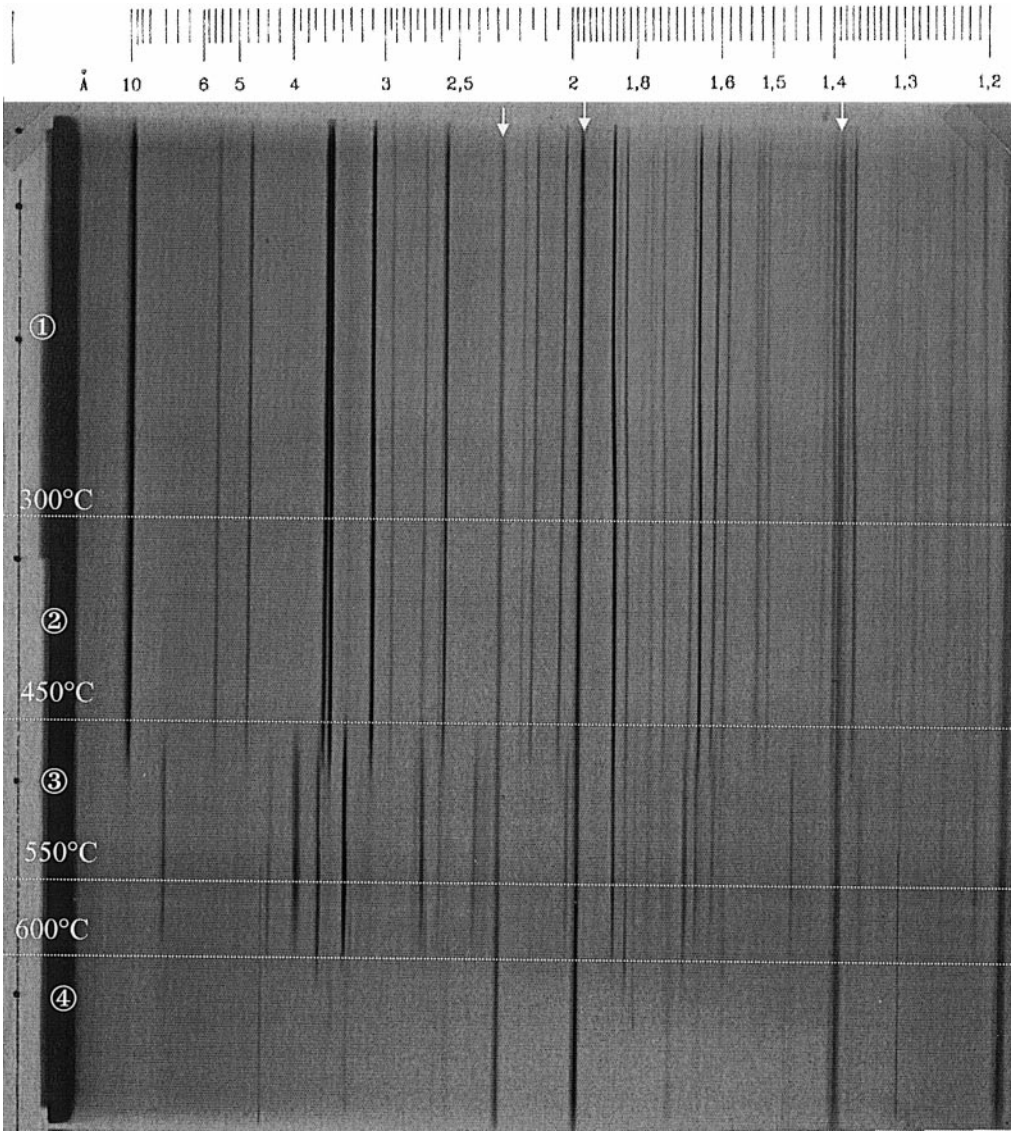

FIG. 2. Guinier–Lenné photograph of $H_{0.13}V_{0.13}Mo_{0.87}O_3 \cdot 0.26H_2O$ (precursor) as a function of temperature. The platinum reflections (standards) are visible at $d = 2.27$, 1.96, and 1.39 Å (white arrows).

oxide irreversibly transforms into a mixed stable orthorhombic MoO_3-type structure oxide $V_{0.13}Mo_{0.87}O_{2.935}$. This chemical formula is deduced from the initial composition of the precursor and from the different weight losses. This transition is characterized, on the DTA curve, by a large asymmetric exothermic peak (Fig. 3, region 3). This peak shape is related to a two-step transition. Upon decreasing the heating rate from 5°C to 1°C/min, the two components could be separated on the DTA curve (Fig. 4). During the TEM study, we will try to explain the origin of the two exothermic peak components.

The unit cell parameters refinement leads to $a = 3.930(2)$ Å, $b = 13.837(2)$ Å, $c = 3.684(7)$ Å. These values relate a slight decrease in the cell parameters, most likely due to the difference in composition, compared to those of the orthorhombic MoO_3 (12): $a = 3.963$ Å, $b = 13.855$ Å, $c = 3.696$ Å. The conditions on the reflections are $h01$ $h + 1 = 2n$ and $0k1$ $k = 2n$, consistent with *Pbnm* space group of orthorhombic MoO_3.

3. *Phase Segregation: Liquid Phase + Orthorhombic MoO_3 Phase*

Around 600°C, the appearance of a liquid phase marks the evolution of the system toward the stable equilibrium of the binary V_2O_5–MoO_3. The temperatures of the phenomena appearing during the heating of the mixed phase are consistent with the values read on the binary system (13)

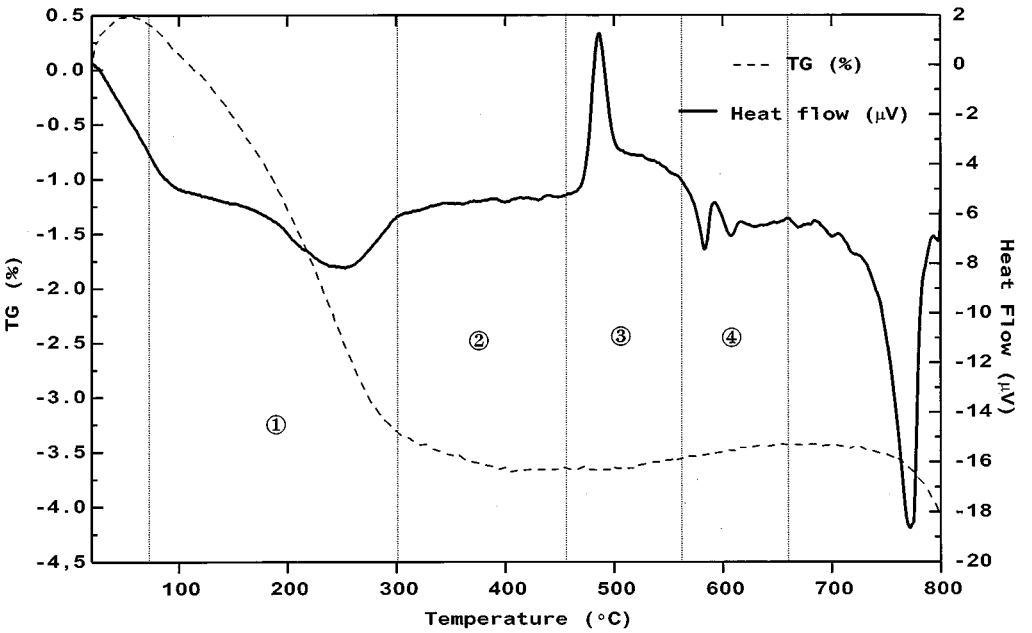

FIG. 3. STA curves obtained from $H_{0.13}V_{0.13}Mo_{0.87}O_3 \cdot 0.26H_2O$ precursor, Ramp (5°C/min).

(Fig. 5), which correspond to eutectic and final melting phenomena. The heating of the orthorhombic mixed oxide around 600°C induces the formation of a liquid phase and a solid phase chemical composition, which tends to MoO_3; around 750°C the fusion is complete. Indeed, the disappearance of the reflections on the X-ray diagram is consistent with this hypothesis. According to the design of the heating room, the sample is laid in vertical position. The liquid

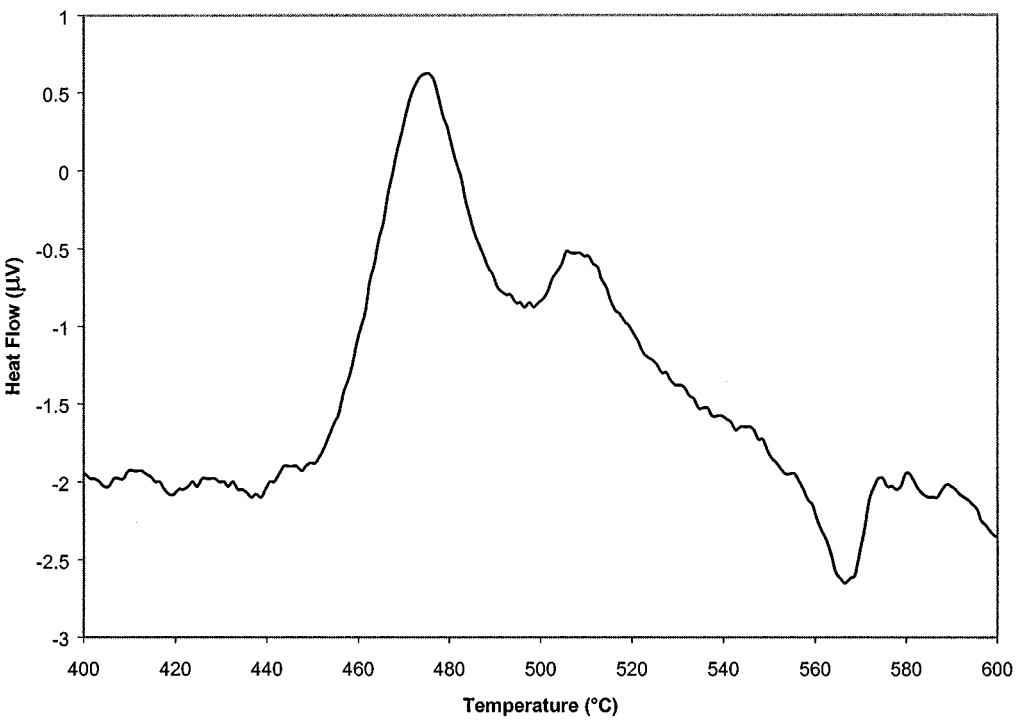

FIG. 4. DTA curve between 400 and 600°C realized from $H_{0.13}V_{0.13}Mo_{0.87}O_3 \cdot 0.26H_2O$ precursor, Ramp (1°C/min).

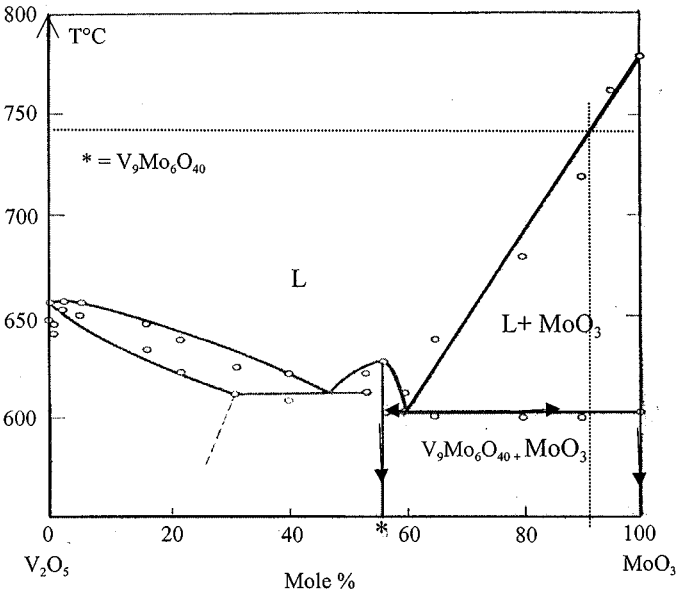

FIG. 5. V_2O_5–MoO_2 binary diagram proposed by Bielanski *et al.* (13); the vertical line corresponds to the studied mixed oxide composition. *Defined compound ($V_9Mo_6O_{40}$, more likely V_2MoO_8). The horizontal line gives the fusion temperature for our phase composition. The arrows indicate the cooling way when the sample is quenched from 600°C to room temperature.

phase resulting in the separation of the powder from the platinum grid, only the platinum reflections remain above 600°C (Fig. 2, region 4). The eutectic phenomenon at 600°C is characterized on the DTA curve by an endothermic peak (Fig. 3, region 4) and the complete fusion by a large endothermic peak at 770°C. According to the binary system, the quenched product from 600°C should be a mixture of $V_9Mo_6O_{40}$ and MoO_3. The TG curve shows a weight gain around this temperature (Fig. 3, region 4) pointing out the formation of fully oxidized phases in this temperature range due to the effect of residual oxygen contained in argon. The $V_9Mo_6O_{40}$ (14) and V_2MoO_8 (15) compounds exhibiting very close unit cell parameters, $a = 19.338$ Å, $b = 3.628$ Å, $c = 4.123$ Å, $\beta = 90.6°$ and $a = 19.398$ Å, $b = 3.629$ Å, $c = 4.117$ Å, $\beta = 90.34°$, respectively, it is difficult to distinguish between them. Contrary to the binary proposed by Bielanski *et al.* (13), we thought that the defined compound could not be the reduced phase $V_9Mo_6O_{40}$. Such a reduced oxide could not form in the binary V_2O_5–MoO_3. Volkov *et al.* (16), who have also studied this binary system, found a solid solution between a defined compound at 50% MoO_3 (V_2MoO_8) and a defined compound at 57.1% MoO_3 ("$V_9Mo_6O_{40.5}$"). Our purpose is not to discuss this problem. For our paper, we will use the V_2MoO_8-type phase term for the 57.1% MoO_3 compound. The segments inverse rule points out that the quantity of V_2MoO_8-type phase would be small in comparison with that of MoO_3 at 600°C. In order to verify this hypothesis, the precursor was put in the middle of a large porcelain crucible, heated at this temperature for 5 h under air in a muffle furnace, and then quenched at room temperature. The amount of "solid" phase decreased and the crucible bottom was stained in yellow due to the step through a liquid phase. The X-ray diffraction pattern (Fig. 6) evidences intense orthorhombic MoO_3-type structure reflections and weak reflections of monoclinic V_2MoO_8-type structure. The unit cell

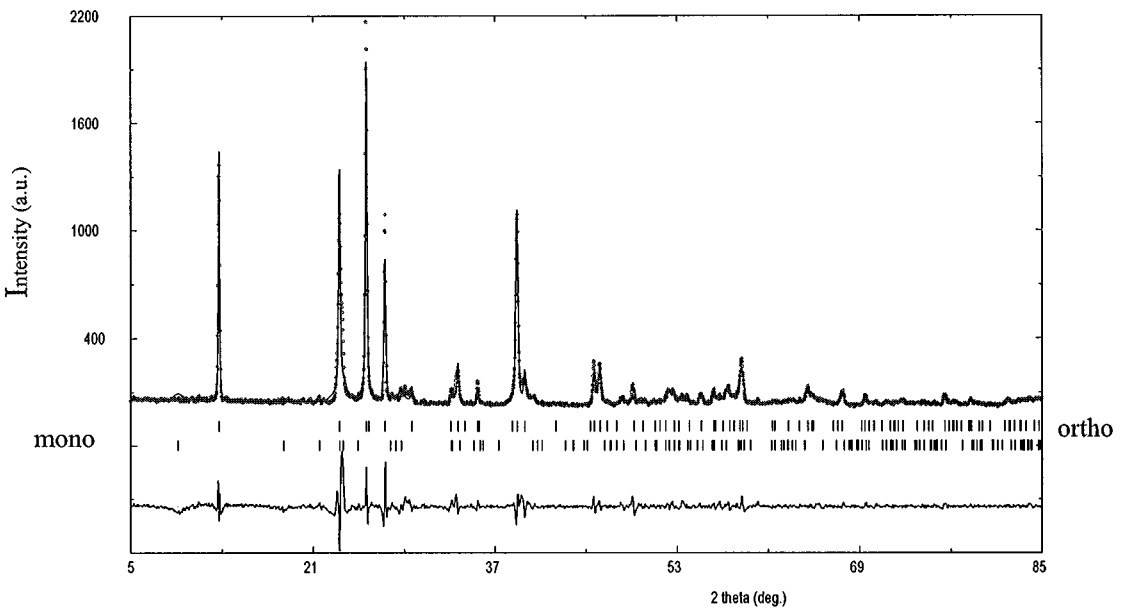

FIG. 6. Experimental and calculated X-ray diffraction patterns obtained from the $H_{0.13}V_{0.13}Mo_{0.87}O_3 \cdot 0.26H_2O$ precursor heated at 600°C for 5 h: mixture of orthorhombic MoO_3 and monoclinic V_2MoO_8-type structure.

parameters of these phases are: for the orthorhombic MoO_3 phase, $a = 3.960(1)$ Å, $b = 13.860(1)$ Å, $c = 3.695(3)$ Å, and for the monoclinic V_2MoO_8-type phase $a = 19.361(5)$ Å, $b = 3.627(2)$ Å, $c = 4.121(1)$ Å, $\beta = 90.80(2)^\circ$. The values are respectively close to the unit cell parameters proposed for orthorhombic MoO_3 (12) and for monoclinic $V_9Mo_6O_{40}$ (14) or V_2MoO_8 (15). So far, we do not know if the vanadium segregation is complete, what the real chemical composition of the formed phases is, and what the reaction mechanism observed during the segregation is.

The TEM study of this transformation will answer these questions.

B. TEM Study of Phase Transition

Due to amorphization and dehydration phenomena under the intense electron beam, the hexagonal MoO_3-type structure phase could not be observed by HREM. Only the electron diffraction and the classical imaging will give information on this phase. The phase transition and phase segregation taking place on a short temperature interval (from 500 to 600°C), all the transformation steps, from the initial hexagonal MoO_3-type mixed oxide particles to the final orthorhombic MoO_3 oxide obtained after phase segregation, will be observed on the same sample (topochemistry concept).

1. Evolution of the Particles Habitus

First, the tips of the initial needles (Fig. 7a) exfoliate (Fig. 7b). After exfoliation, the habitus is completely transformed. The needles become larger (stick shape). The transformation continues, the sticks become larger and larger and thinner and thinner. A thinning down of the initial stick

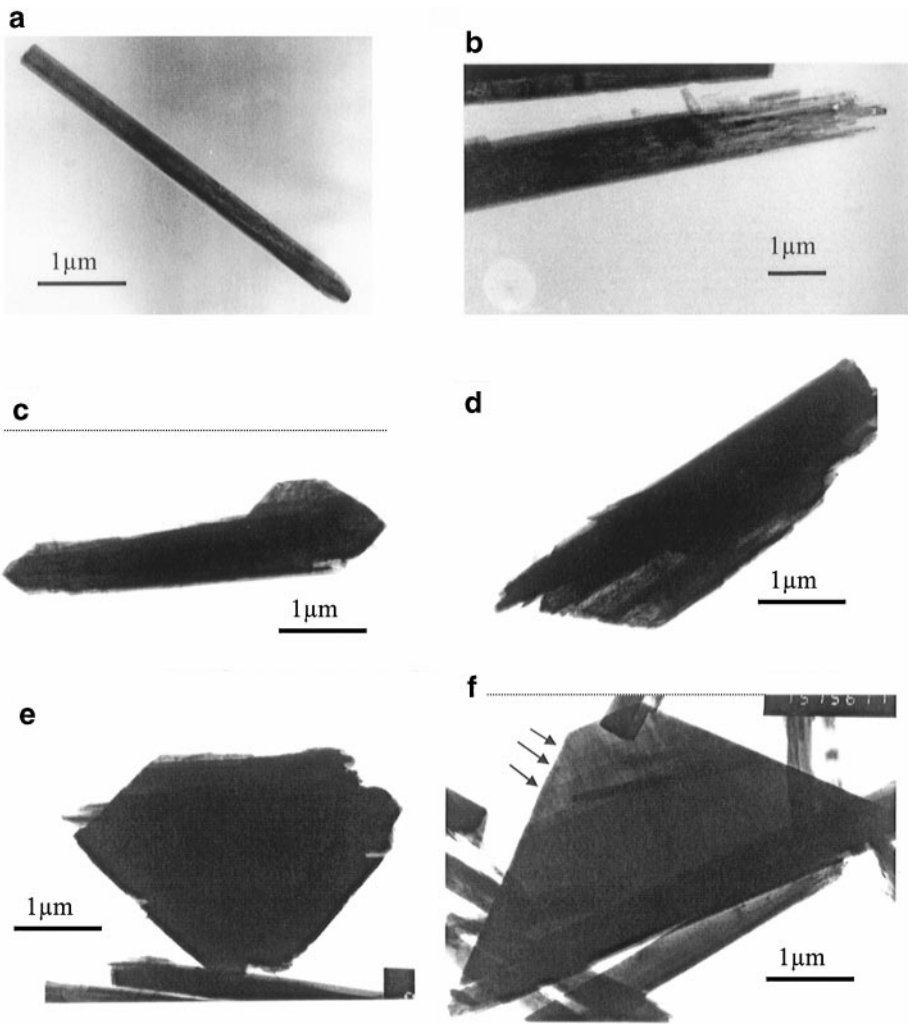

FIG. 7. Evolution of the particles habitus during the phase transitions. (a) Initial needle of $H_{0.13}V_{0.13}Mo_{0.87}O_3 \cdot 0.26H_2O$; (b) Exfoliated needle of $H_{0.13-x}V_{0.13}Mo_{0.87}O_{3-x/2}$; (c) stick of $V_{0.13}Mo_{0.87}O_{2.935}$, the segregation has begun; (d and e) growth of the platelet of MoO_3 on the $V_{0.13}Mo_{0.87}O_{2.935}$ stick; (f) final platelet of MoO_3, matter coat growth limits noted with black arrows.

(Figs. 7c, 7d, and 7e) due to a material transport through a gliding process is observed resulting in thin platelets. Fig. 7f shows the matter coat growth limits. According to higher temperature samples, the platelet shape is the final stage; no additional thinning is observed. Let's now discuss, on the basis of the obtained data, the first observed transformation together with the structural changes inducing the needles tips exfoliation and the formation of the sticks.

2. *Phase Transition between Hexagonal Mixed Oxide and Orthorhombic Mixed Oxide* ($H_{0.13}V_{0.13}Mo_{0.87}O_3 \rightarrow V_{0.13}Mo_{0.87}O_{2.935}$)

a. Selected area electron diffraction pattern (*SAED*) *and EDS analysis X*. All the crystals having a global needle or stick shape show the initial vanadium/molybdenum ratio of the hydrated precursor (0.13/0.87).

A reciprocal space reconstruction was made on the exfoliated needles (Fig. 8). The ED patterns obtained by rotation along the c^*_{hexa} axis (Fig. 8) evidence three linked reflections systems with different intensities. The strong reflections are in good agreement with the hexagonal MoO_3-type cell reflections $a = 10.6$ Å, $c = 3.7$ Å (Fig. 8, filled dots). The second reflections system (Fig. 8, empty dots) forms concentric circles which radii are equal to different interreticular distances of the hexagonal phase. The rings 010, 110 and 020 are stressed. Finally, the third weak spots class results from the double diffraction of the first two systems (Fig. 8, black crosses).

These rings could be brought out only by the reciprocal space reconstruction. Indeed, the relationships between the crystallographic and habitus data (c axis of the hexagonal cell parallel to the long axis of the needles) (6) make SAED observations impossible along the c^* axis. Microdomains form from the monocrystalline needles (monolithe particles). During the transformation, the microdomains remain oriented parallel to the long axis of the needles (c axis). Along other orientations these domains are disoriented and lead to the observation of rings on the reconstruction. This disorientation involves the multiple diffraction phenomenon too.

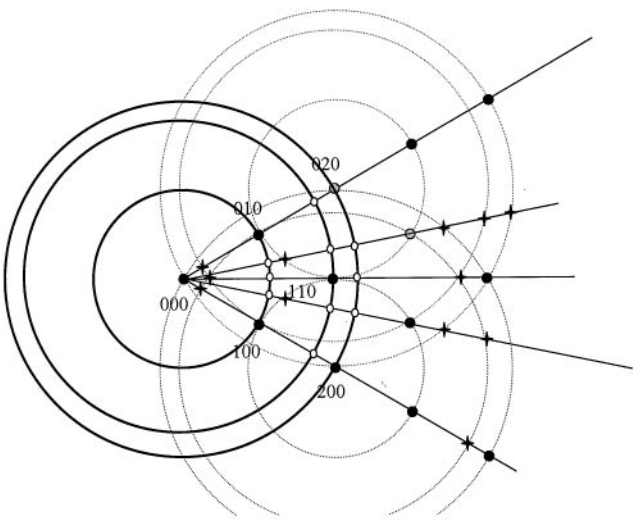

FIG. 8. Reciprocal space reconstruction along c^* axis, carried out on an exfoliated needle, showing supplementary reflections (compared to an initial hexagonal mixed oxide hydrate needle) and explaining their origins.

The first step of the transformation goes through the creation of a polymicrocrystalline particle which domains show a common axis. The particle texture could be related to the "fibrous texture." (This last point is consistent with the observation of exfoliation in conventional TEM).

Then, the exfoliated needle width becomes larger, and a laminated texture inherent to the double layer oxide formation is observed. The widening occurs from only one couple of parallel (010) faces of the needles. The so-formed $V_{0.13}Mo_{0.87}O_{2.935}$ stick should show a preferential orientation along the b_{ortho} axis due to this anisotropy (Fig. 9b). According to the *Pbnm* space group of the orthorhombic MoO_3-type structure, the theoretically forbidden reflections 001 $l = 2n + 1$ and $h00$ $h = 2n + 1$ are observed on the pattern. Two hypotheses could explain this phenomenon. The first one is based on the particle width (more than one micron) and its preferential orientation; given the small b^* axis, a significant form effect induces the upper layer reflections observation. The second one assumes a decrease in the symmetry compared to that of the orthorhombic MoO_3 reference phase; this last hypothesis will be retained according to the results of the HREM study.

The electron diffraction study leads to supplementary information on how the polycrystalline particle transforms into the double layer mixed oxide stick. Orientation relationships could be deduced from the electron diffraction patterns (Figs. 9a and 9b). Figure 9a shows intense spots indexed with orthorhombic unit cell parameters and weak spots with the hexagonal unit cell parameters. The $h01$ $h + 1 = 2n$, h odd reflections are missing. The orthorhombic MoO_3-type structure mixed oxide nucleates, and only a few plans are formed. Conversely, Fig. 9b is a monophasic electron diffraction pattern realized on a pure $V_{0.13}Mo_{0.87}O_{2.935}$ stick. However, supplementary spots could not be indexed with the orthorhombic or the hexagonal cell parameters. These reflections could be explained according to the two hypotheses given above and to the HREM observations.

In summary, the transition between the hexagonal and the mixed orthorhombic phases occurs through intermediary phases with destruction of the monolithic particle, creation of fibrous needle, and then reconstruction of the double layer mixed oxide stick. All along the transformation, the crystallographic relationship [001] hexagonal//

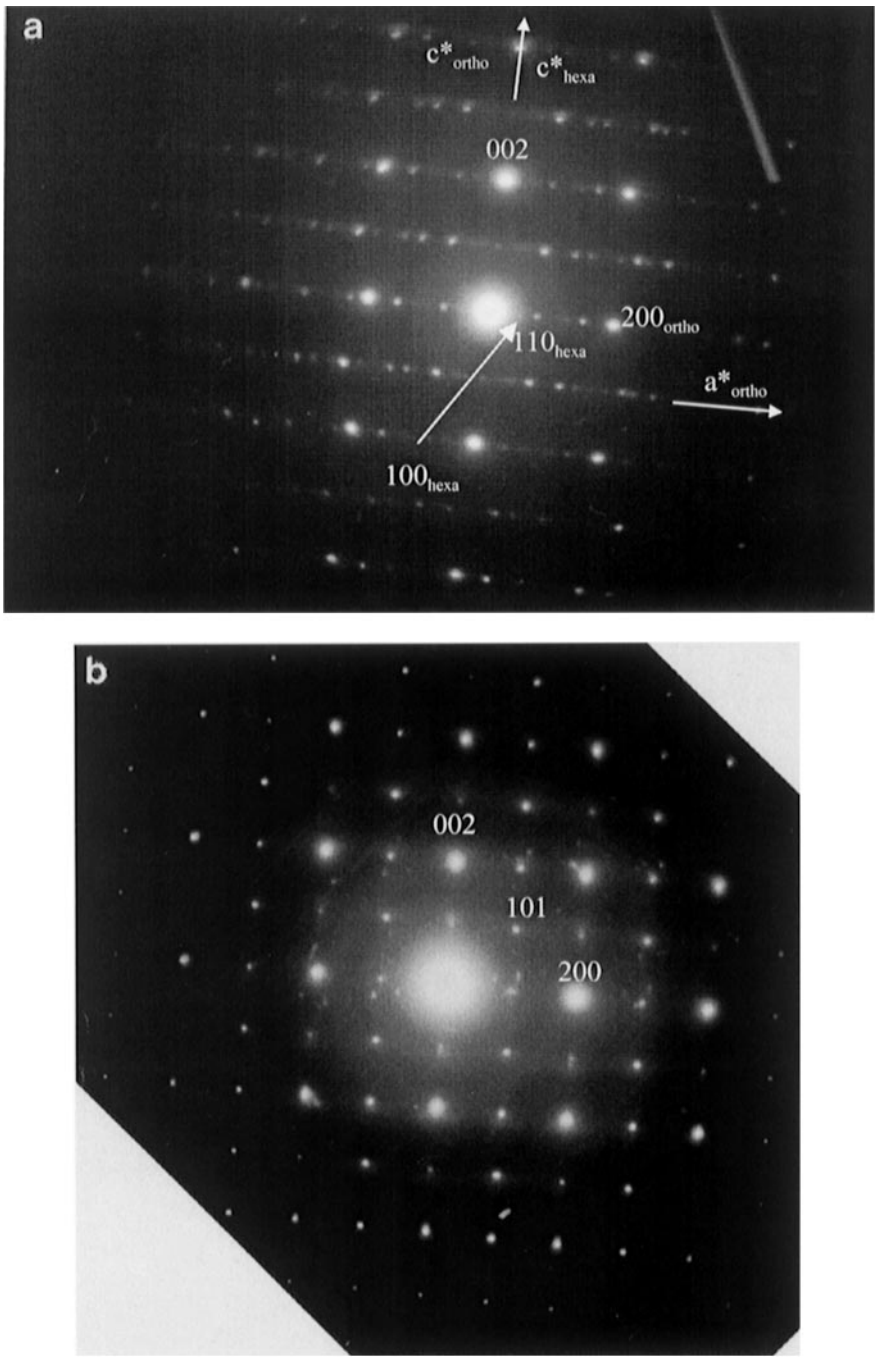

FIG. 9. Electron diffraction pattern along [020] direction of the orthorhombic mixed oxide taken on an exfoliated needle transforming into a stick. (a) Nucleation of the orthorhombic double layer mixed oxide on polymicrocrystallites, (b) monophasic SAED of the double layer mixed oxide $V_{0.13}Mo_{0.87}O_{2.935}$.

[001] orthorhombic is kept. This transformation by first destruction of the initial structure and then reconstruction of the new structure enlightens us on the two components of the large exothermic peak observed around 500°C on the DTA curve (Fig. 3).

b. HREM study of orthorhombic mixed oxide $V_{0.13}Mo_{0.87}O_{2.935}$ *along* [010]. Along this direction, the double layer structure is observed perpendicularly to the layers. Figure 10 is an image taken at Scherzer defocus on the edge of an orthorhombic mixed oxide stick. For Scherzer defocus, the

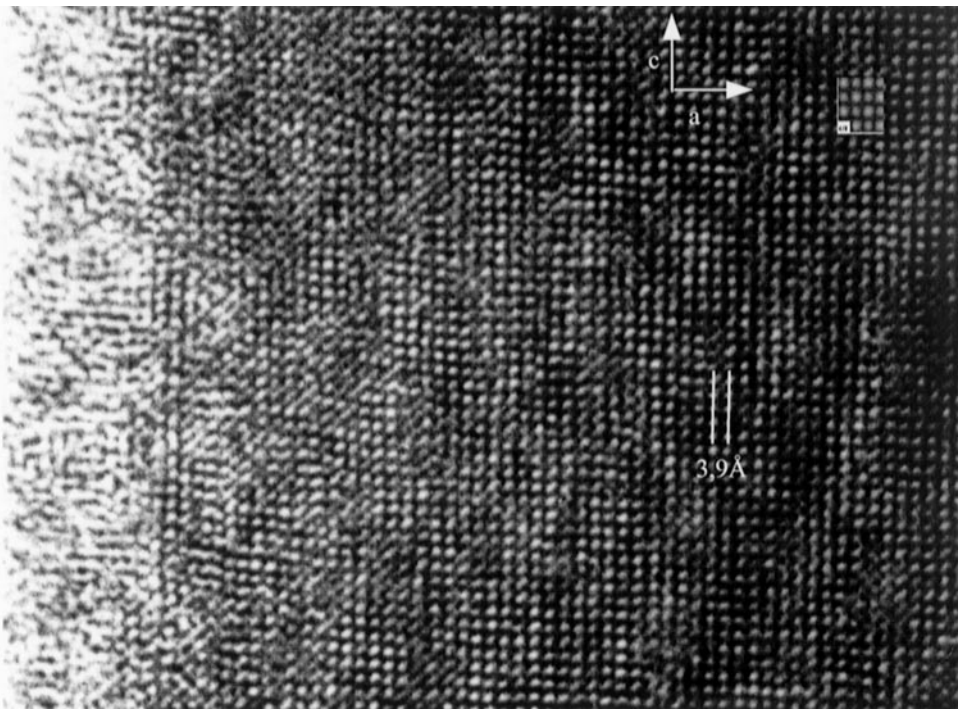

FIG. 10. HREM image of the orthorhombic mixed oxide $V_{0.13}Mo_{0.87}O_{2.935}$ along [010].

white dots correspond to the less electronic density zones. The chemical V/Mo composition was checked and proves that the ratio V/Mo remains equal to 0.13/0.87. The contrast is made by white dots in the thicker region, spaced 3.9 Å, in a square array. The image simulation, calculated with the atomic positions of orthorhombic MoO_3 by substituting 13% of the molybdenum by vanadium for a thickness of 60 Å and a defocus of -500 Å, is on the top right of the image. (It is difficult to directly fit the observed contrast with the projected structure due to the imperfect projection of the atom's layers along this direction).

Contrast variations are observed on the picture. On the edge of the particle, the dots stretch at 45° of the *c* axis. This stretching corresponds to the resolution of the heavy atoms of the inferior layer, which are not vertical with the atoms of the superior layer. Viewing the image at grazing incidence, the white dot rows are not linear. The observed modulations are not commensurable. This row's ripple is caused by a slight displacement in the atomic positions (compared to the type structure), which induces a decrease in the symmetry. Then, the observed reflections, forbidden by the

TABLE 1
Punctual EDS Analysis on the Mixed Oxide Stick Transforming into MoO_3 Platelet of Fig. 1

Analysis point	Vanadium			Molybdenum		
	Weight %	Sigma %	Atomic %	Weight %	Sigma %	Atomic %
Point 1	5.83	0.38	10.45	94.17	0.38	89.55
Point 2	1.81	0.30	3.35	98.19	0.30	96.65
Point 3	1.36	1.43	0	98.64	1.43	100

Note. The analysis point numbers refer to the location numbers noted on Fig. 11.

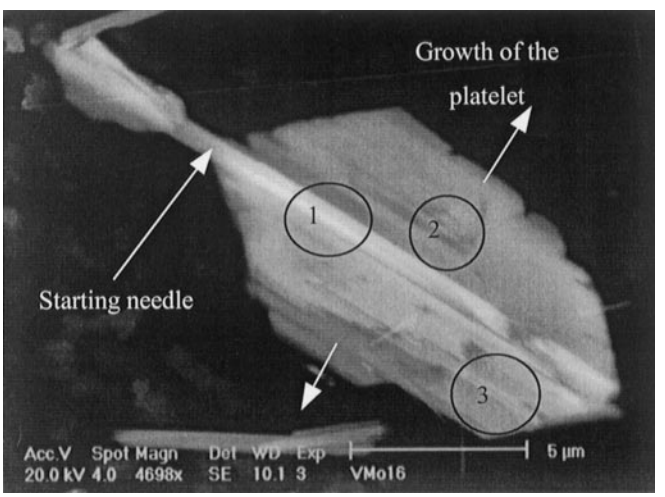

FIG. 11. SEM image of an orthorhombic mixed oxide $V_{0.13}Mo_{0.87}O_{2.935}$ stick transforming in a MoO_3 platelet during the phase segregation.

space group *Pbnm* of MoO_3, are induced not only by the form effect but also by the local distortion of the structure decreasing the symmetry.

The reaction carries on, the mixed orthorhombic oxide could be considered as an intermediary phase. Segregation occurs if the heating is extended. During this segregation, a liquid phase with the composition 60% MoO_3, 40% V_2O_5 and a solid pure orthorhombic phase are formed (Fig. 5). The study of this segregation, linking the liquid phase departure from the crystal and the impoverishment of the crystal in vanadium with the habitus evolution and the local microstructure, is presented below.

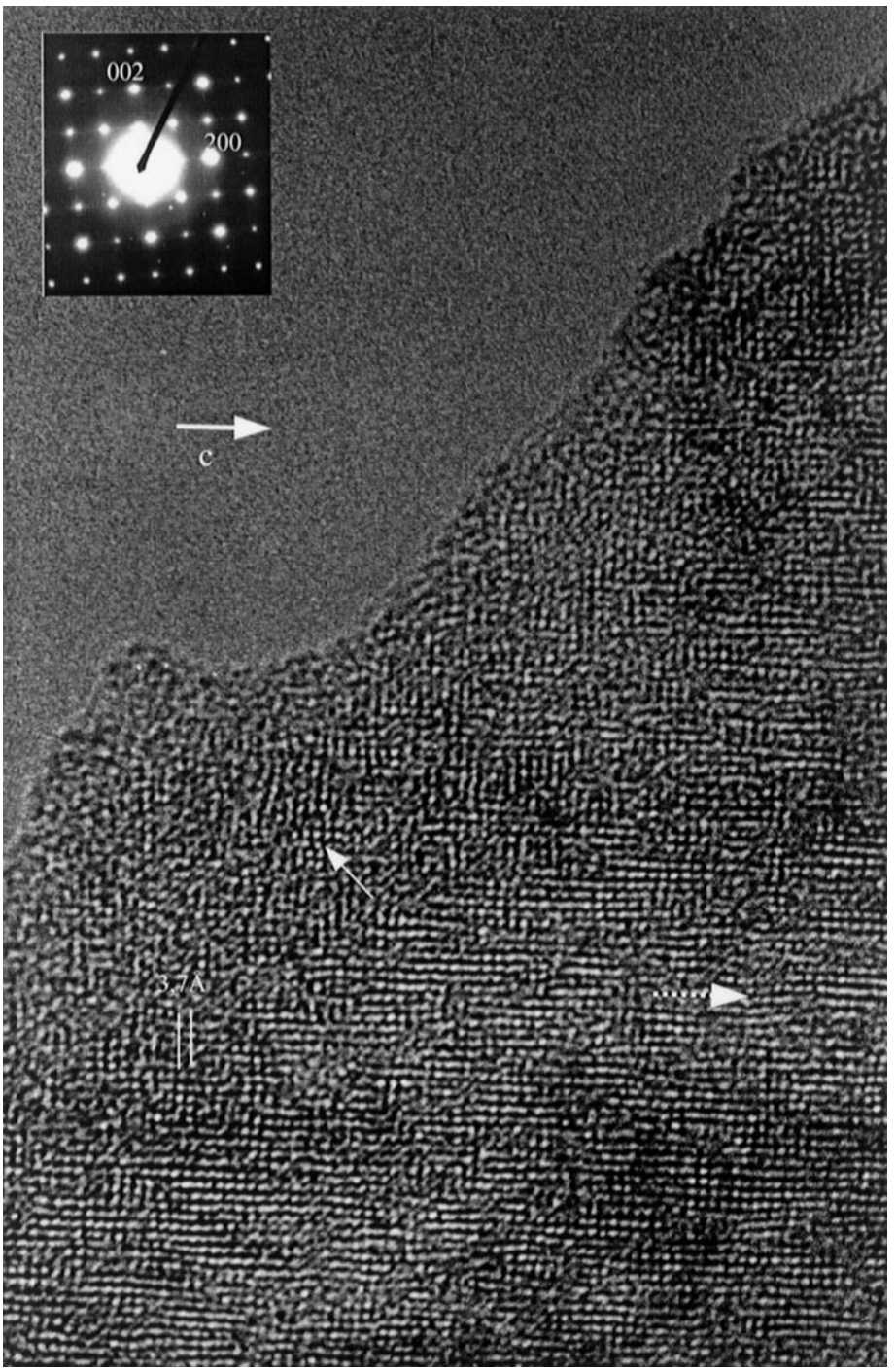

FIG. 12. HREM image of the final orthorhombic MoO_3 platelet along [010].

3. *Study of the Phase Segregation ($V_{0.13}Mo_{0.87}O_{2.935} \rightarrow V_2MoO_8$-Type Phase + MoO_3)*

a. Habitus evolution versus chemical composition. In these samples, the observed particles show an intermediary habitus between the stick and the platelet. A preliminary study by EDS on a TEM revealed a variation in the vanadium concentration versus location of the probe on the particle. An EDS mapping of the particle was carried out in a SEM (Fig. 11). The vanadium amount decreases quickly to zero when the probe is moved from the middle to the edge of the particle. Different analysis points are reported in Table 1.

All the vanadium leaves the particle through the liquid phase. This one generates a displacement of the solid matter and creation of the platelet. The growth is parallel to one plane. No twin domains are observed around the initial stick region. The SEM image shows the puff texture of the platelet intuited during the TEM study. Moreover, such an image shows where the nucleation takes place. The middle of the particle is the last part to transform. No half-stick sliding is observed, the sliding occurs layer by layer on the surface. A theoretical reactional mechanism in agreement with the phase segregation and the observed phenomena is proposed below.

b. Proposed reactional mechanism. The initial $V_{0.13}Mo_{0.87}O_{2.935}$ sticks preferentially lie on the (010) plane. The layers of the structure are parallel to this plane. Segregation between the vanadium and the molybdenum takes place. The vanadium goes away from the structure with some neighboring molybdenum and oxygen atoms. The minority species (vanadium) amount decreases in the double layers.

This liquid soup vanadium/molybdenum/oxygen accumulates between the layers. Then, the bonds between two adjacent layers break. The liquid phase separates the solid matrix, and the thin solid layer slides toward the edge of the particle. The stick gradually transforms into a platelet through a slicing of layers. The transformation starts at the surface and extends to the particle middle. This mechanism stops when the particle composition is MoO_3.

According to this mechanism, local structure variation inducing an increase in the faults in the final particle microstructure must be observed. The HREM study is reported below.

c. HREM observation of the final orthorhombic MoO_3 platelet. Figure 12 is an image of the final particle along [010]. The corresponding SAED is reported also. The supplementary reflections and diffuse bands are observed. The comparison between the image contrasts before and after segregation shows an increase in disordered microstructure. Only a few "well" crystallized domains of three or four cells wide remain (white arrows). This image is in good agreement with the proposed mechanism.

CONCLUSIONS

The thermal treatment performed on the hydrated precursor $H_{0.13}V_{0.13}Mo_{0.87}O_3 \cdot 0.26H_2O$ creates new metastable and stable oxides. Among these oxides, the mixed oxides $H_{0.13-x}V_{0.13}Mo_{0.87}O_{3-x/2}$ $(0 \leq x \leq 0.13)$ isostructural with hexagonal MoO_3 and orthorhombic $V_{0.13}Mo_{0.87}O_{2.935}$ could be isolated. The electron diffraction and TEM studies show that the transition induces a change in the habitus of the particle. The initial monolithic needle is partially destroyed and becomes mosaic (polycrystalline). The crystallites remain parallel to the long axis of the particle. The nucleation of the orthorhombic mixed oxide took place on these crystallites. At the end of the transition, the particle exhibits a large stick shape. Finally, a phase segregation inducing the transformation of the previous stick in a badly crystallized orthorhombic MoO_3 platelet was observed.

ACKNOWLEDGMENTS

The authors thank Ms. Sunberg and Ms. Hervieu for their scientific discussions. L. Dupont thanks the Department of Inorganic Chemistry Stockholm University and CRISMAT laboratory of ISMRA and University of Caen for their hospitality.

REFERENCES

1. T. P. Feist and P. K. Davies, *in* "Chemistry of Electronic Ceramic Materials, Proceedings of an International Conference Held in Jackson Hole, WY," p. 163. 1987.
2. Y. Hu, P. K. Davies, and T. P. Feist, *Solid State Ionics* **53–56,** 539 (1992).
3. T. P. Feist and P. K. Davies, *Chem. Mater.* **3,** 1011 (1991).
4. J. Galy, J. Darriet, and B. Darriet, *C. R. Acad. Sci. Paris C* **264,** 1477 (1967).
5. Y. Hu and P. K. Davies, *J. Solid State Chem.* **105,** 489 (1993).
6. L. Dupont, D. Larcher, F.Portemer, and M. Figlarz, *J. Solid State Chem.* **121,** 339 (1996).
7. A. Boultif and D. Louër, *J. Appl. Crystallogr.* **5,** 24 (1991).
8. A. D. Mighell, C. R. Hubbard, and J. K. Stalick, "NBS*AIDS80: A Fortran Program for Crystallographic Data Evaluation," Technical note 1141. National Bureau of Standards, Washington, DC, 1981. [NBS*AIDS83 is an expansed version of NBS*AIDS80].
9. J. Rodriguez-Carjaval. "Collected Abstracts of Powder Diffraction Meeting, Toulouse France" (J. Galy, Ed.), p. 127. 1990.
10. P. Stadelmann, http://cimewww.epfl.ch/CIOLS/crystal1.pl.
11. J. Guo, P. Zavalij, and M. S. Whittingham, *Eur. J. Solid State Inorg. Chem.* **31,** 833 (1994).
12. N. Wooster, *R. Krist.* **80,** 504 (1931).
13. A. Bielanski, K. Dyrek, J. Pozniczek, and E. Wenda, *Bull. Ac. Pol. Sci.* **XIX**(8), 507 (1971).
14. R. C. T. Slade, A. Ramanan, B. C. West, and E. Prince, *J. Solid State Chem.* **82,** 65 (1989).
15. H. A. Eick and L. Kihlborg, *Acta Chem. Scand.* **20,** 1658 (1966).
16. B. M. Volkov, R. Tynkacheva, A. Iotiev, and E. Tkachenko, *Russ. J. Inorg. Chem.* **17**(10), 2803 (1972).